



AN3973

Application note

Electronic ballast with active PFC using STD3N62K3 power MOSFET and STD845DN40 BJT device

Introduction

In the most recent developments regarding energy saving, optimization and correct selection of design components are considered a must in order to have improved electric efficiency. An increasing sensitivity regarding energy problems has made companies and consumers more demanding. In this context, cooperation and support between silicon makers and customers is paramount: an exchange of experience leads to a better and quicker way to realize new projects. In this article, we present an electronic ballast project designed thanks to customer input. This application note describes the demonstration board for 2X28 W electronic lamp ballast with active PFC. The ballast is formed by a part of the PFC section and a self-oscillating half bridge converter. The circuit has been designed for a nominal input voltage of $230\text{ Vrms}\pm15\%$ and 50-60 Hz. The key components are the power bipolar transistor (STD845DN40), the MOSFET device (STD3N62K3), and an ST power switching driver for the PFC section. The purpose of this application note is to show a simple and cheap lighting application optimized in terms of power factor (PFC), THD harmonic distortion, and electric efficiency. The DC-AC converter section presents a layout solution that offers the customer the possibility of using a bipolar transistor, or DIP 8 or SOT-82 package.

Contents

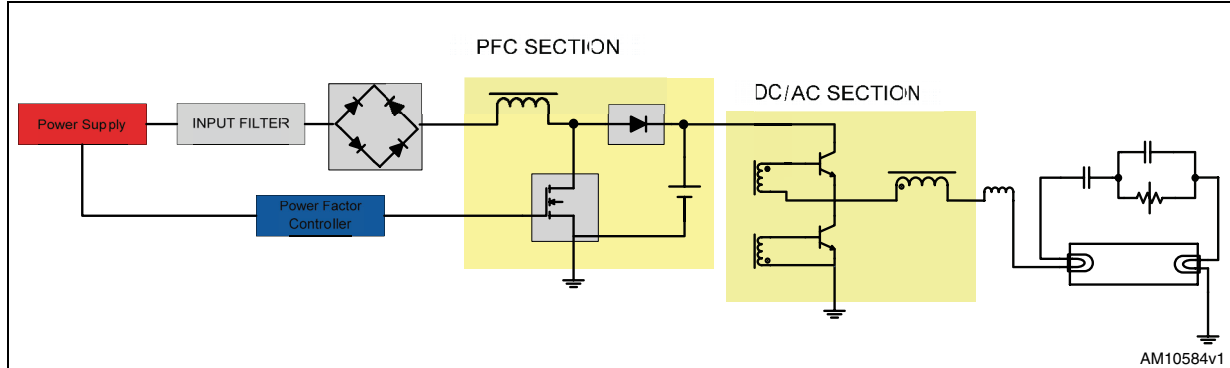
| | | |
|-----------|-----------------------------|-----------|
| 1 | System description | 4 |
| 2 | Power factor section | 5 |
| 2.1 | PFC section design | 6 |
| 2.1.1 | Input capacitor | 7 |
| 2.1.2 | Output capacitor | 7 |
| 2.1.3 | Boost inductor | 7 |
| 2.1.4 | Power MOSFET selection | 7 |
| 2.1.5 | L6562A biasing circuitry | 8 |
| 3 | DC-AC converter | 10 |
| 3.1 | System description | 11 |
| 3.1.1 | Preheating phase | 11 |
| 3.1.2 | Ignition phase | 12 |
| 3.1.3 | Steady-state phase | 13 |
| 4 | Driving optimization | 14 |
| 4.1 | MOSFET circuit optimization | 14 |
| 4.2 | BJT circuit optimization | 16 |
| 5 | Experimental results | 18 |
| 6 | Conclusions | 19 |
| 7 | Layout layers | 20 |
| 8 | Bill of material | 21 |
| 9 | Reference | 22 |
| 10 | Revision history | 23 |

List of figures

| | | |
|------------|--|----|
| Figure 1. | Ballast model | 4 |
| Figure 2. | PFC section, boost converter diagram | 5 |
| Figure 3. | Inductor and input current waveform. MOSFET timing | 6 |
| Figure 4. | PFC section, relevant elements for THD and PFC factor | 8 |
| Figure 5. | DC-AC converter section | 10 |
| Figure 6. | Voltage and current lamp waveforms | 12 |
| Figure 7. | Zoom of the highlighted section (in <i>Figure 6</i>) | 12 |
| Figure 8. | Voltage and current lamp waveforms | 12 |
| Figure 9. | Zoom of the highlighted section (in <i>Figure 8</i>) | 12 |
| Figure 10. | Voltage and current lamp waveforms | 13 |
| Figure 11. | Zoom of the highlighted section (in <i>Figure 10</i>) | 13 |
| Figure 12. | Snubber and driving circuit of MOSFET | 14 |
| Figure 13. | MOSFET turn-off without snubber circuit | 15 |
| Figure 14. | MOSFET turn-off with snubber circuit | 15 |
| Figure 15. | MOSFET turn-on @ R ₇ =10 W | 15 |
| Figure 16. | MOSFET turn-on R ₇ =47 W | 15 |
| Figure 17. | BJT in low side. Snubber and driving circuit of BJT | 16 |
| Figure 18. | Steady-state operation | 16 |
| Figure 19. | Zoom of the highlighted section 1 (in <i>Figure 18</i>) | 17 |
| Figure 20. | Zoom of the highlighted section 2 (in <i>Figure 18</i>) | 17 |
| Figure 21. | Bottom layout layer | 20 |
| Figure 22. | Top layout layer | 20 |
| Figure 23. | Silkscreen top | 20 |
| Figure 24. | Silkscreen bottom | 20 |

1 System description

Figure 1. Ballast model



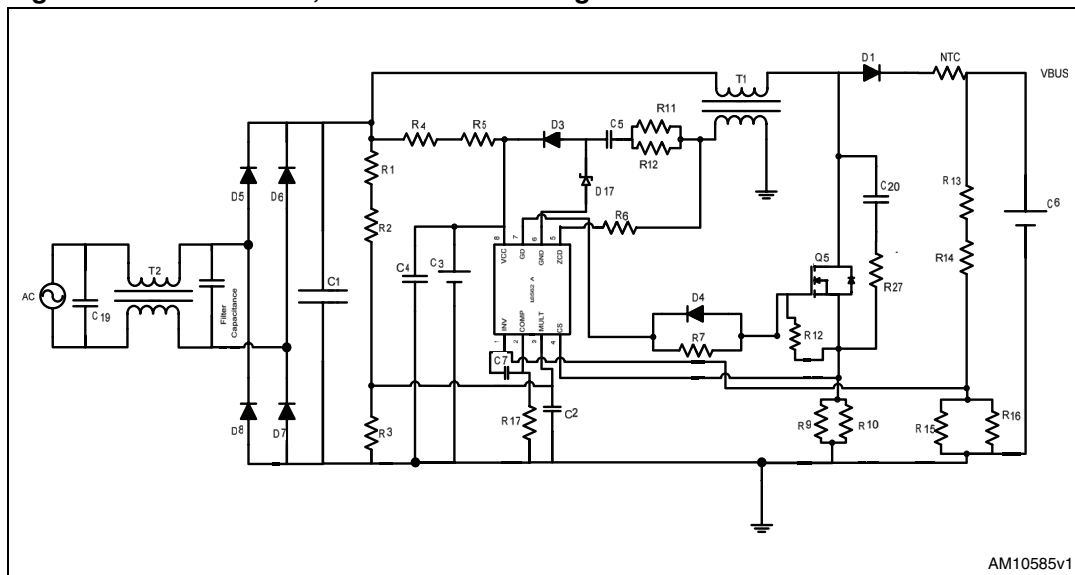
The system description is subdivided into two main sections, namely the PFC boost section and half bridge converter. The system description starts with the PFC section and then continues with the DC-AC converter. In the PFC section the method and the electrical elements concerning the optimization of PFC and THD parameters are pointed out. In the DC-AC converter section, the focus is the optimization of transistor bipolar driving.

2 Power factor section

The PFC section (boost converter) mainly consists of STD3N62K3 MOSFET SuperMESH3 technology and the L6562A power switching driver. The new SuperMESH3 technology is obtained through the combination of fine tuning between standard SuperMESH and MDMESH technology. This has resulted in the development of a new technology that represents the optimization of the basic standard SuperMESH in terms of $R_{DS(on)}^*$ area and dynamic features. SuperMesh has integrated Zener diodes gate-to-source in order to protect its gate-oxide from voltage spikes. The L6562A is a current-mode PFC controller operating in transition mode. It has an improved performance compared to its predecessor, the L6561.

Figure 2 shows the PFC section schematic plus the component values.

Figure 2. PFC section, boost converter diagram



The power factor consists of the displacement factor related to phase angle and the distortion factor related to wave shape. The displacement factor is the ratio between the real power (transferred to the output) and the apparent power (RMS line voltage times RMS line current) drawn from the main, while the distortion factor is the ratio between the fundamental component of the current and the total current:

Equation 1

$$PF = \frac{I_{rms} V_{rms} \cos \theta}{I_{rms} V_{rms}} * \frac{I_{rms_i}}{I_{rms_T}} = \frac{I_{rms_i}}{I_{rms_T}} \cos \theta = K_d * K_\theta$$

Therefore, the section is designed in order to minimize input current distortion and forces the input current to be in phase with the input voltage.

This system operates in transition mode, the boundary between continuous and discontinuous current mode. The control simplicity and the inductor size, due to the low inductance value needed, are the main advantages of this conduction current mode.

2.1 PFC section design

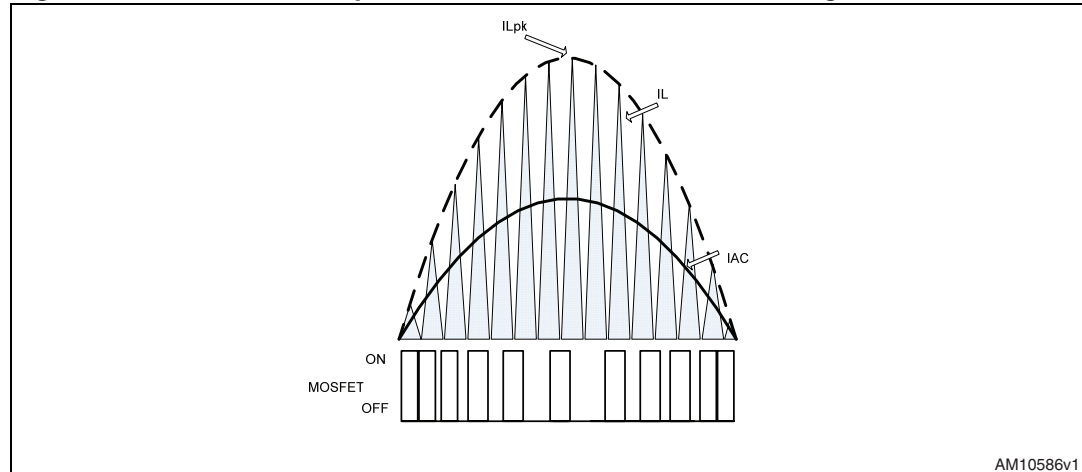
The first step is to define the converter specifications that the user must set for the new PFC boost topology project.

Table 1. Converter specification data and fixed parameters

| Name | Symbol | Value |
|-----------------------------|---------------------------|--------------------|
| Input voltage range | V_{INmin} - V_{INmax} | 180 Vac to 264 Vac |
| Nominal output voltage | V_{out} | 400 V |
| Nominal output power | P_{out} | 60 W |
| Target efficiency | η | ~ 90% |
| Minimum switching frequency | f_s | 35 kHz |
| Expected power factor | PF | 0.99 |

At switching frequency, the inductor current is a triangle shape and the average value is half of the peak of triangle. The resulting inductor current is shown in [Figure 3](#), where it is also shown that, by geometric relationships, the average value is the peak of sinewave input current. The system operates the boundary between continuous and discontinuous (transition mode current):

Figure 3. Inductor and input current waveform. MOSFET timing



Therefore the main operating conditions are:

- RMS input current $I_{in} = \frac{P_{in}}{\sqrt{V_{ACmin}PF}} = \frac{P_{out}}{\eta * V_{ACmin}PF} = 0.374A$
- Peak inductor current $IL_{pk} = 2\sqrt{2}I_{in}$
- RMS inductor current $IL_{RMS} = \frac{2}{\sqrt{3}}I_{in}$

2.1.1 Input capacitor

The input filter capacitor (C_{in}) must reduce the high frequency voltage ripple across C_{in} and the switching noise due to the high frequency inductor current ripple. The input capacitor depends on the voltage ripple (r) and it is usually between 5% and 20% of the minimum input voltage:

- Ripple voltage coefficient (%): $r = 0.1$
- Input capacitor $C_{IN} = \frac{I_{in}}{2\pi f_{SW\min} * V_{AC\min} * r} \approx 100\text{nF}$

In the applicative conditions, a polyester capacitor was chosen. It offers benefits in terms of voltage stability and power factor (PF).

2.1.2 Output capacitor

The output capacitor is a function of voltage ripple (ΔV_{out}) and of the capacitor impedance. ΔV_{out} is usually selected at around 1.5% of the output voltage capacitor:

- Output capacitor $C_{Out} = \frac{P_{out}}{4\pi f_{main} * V_{out} \Delta V_{out}} \approx 47\mu\text{F}$

An electrolytic capacitor has been selected because it has low impedance (ESR) and therefore provides good energy storage and improves the transient performance.

2.1.3 Boost inductor

The inductor boost depends on the several parameters and different approaches which can be used. First, the inductor value is usually calculated so that the minimum switching frequency is greater than the maximum frequency of the L6562A internal starter. Assuming unity PF, it is possible to write:

- Instantaneous switching frequency $f_{sw} = \frac{1}{2LP_{IN}} \frac{V_{AC}^2(V_{out} - \sqrt{2}V_{AC} \sin(\theta))}{V_{out}}$

Therefore, the inductor value is determined at the top of the sinusoid ($\theta = \frac{\pi}{2}$) where the switching frequency is the minimum:

- Inductor value $L(V_{AC}) = \frac{V_{AC}^2(V_{out} - \sqrt{2}V_{AC})}{2f_{SW\min} V_{out} * P_{IN}}$

The optimum dynamic performances of the MOSFET device, selected for this application, have allowed higher operation minimum frequency and consequently lower boost inductance. In this case a 1.8 mH boost inductance was selected.

2.1.4 Power MOSFET selection

MOSFET SuperMESH3 technology perfectly matches boost converter characteristics. In fact, this technology has got a dynamic performance better than that of the standard SuperMESH but not as good as MDMESH. That translates into having low switching power losses and commutation which is not so fast that it implies ringing phenomenon such as decreased PF and THD factors. MOSFET selection is based mainly on maximum voltage rating, total power losses, and maximum operating temperature. In this case a MOSFET device with minimum voltage rating 500 V ($1.2*V_{BUS}=480$ V) must be selected: 20% of V_{BUS}

indicates the safe margin. In the end, the MOSFET selection depended on power losses and maximum operating temperature. MOSFET total power losses depend on conduction and switching losses. The conduction losses at minimum input voltage are calculated by:

- Conduction losses $P_c = R_{DS(on)} \cdot I_{SWrms}^2$

- RMS switch current $I_{SWrms} = I_{Lpk} \text{sen}\theta * \sqrt{\frac{V_{BUS} - \sqrt{2}V_{inmin} \text{sen}\theta}{3V_{BUS}}}$

The switching losses in the MOSFET occur only during turn-off, because this boost topology works in transition mode. Basically they can be expressed by:

- Switching power losses $P_{sw} = \frac{Q_{gd} * V_{BUS} * I_{L_{RMS}}}{2 * I_g} f_s(I_{L_{RMS}})$

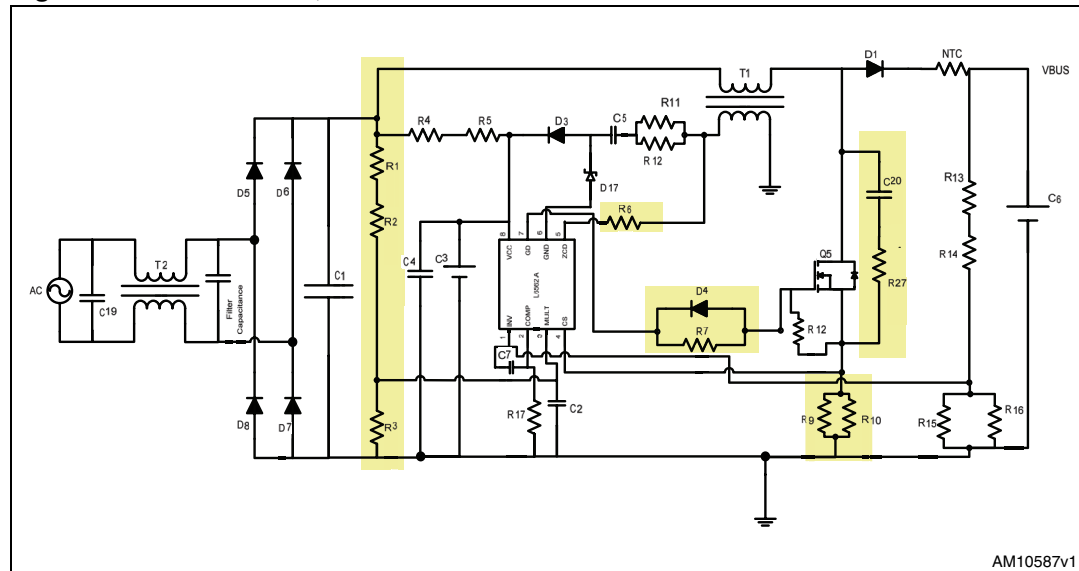
where Q_{gd} is the gate drain charge, $I_{L_{RMS}}$ is RMS inductor current, I_g is the gate current and $f_s(I_{L_{RMS}})$ is switch frequency calculated for value.

Based on the information above, the MOSFET choice was the STD3N62K3 device. The final results show that STD3N62K3 ensures good performance in terms of electrical and thermal behavior.

2.1.5 L6562A biasing circuitry

The dimensioning of biasing circuitry of the L6562A driver is reported for only a few elements. In particular, the dimensioning is shown for those components that have been relevant in terms of THD harmonic distortion and power factor (PF).

Figure 4. PFC section, relevant elements for THD and PFC factor



Pin2 (COMP). A feedback compensation network is put between this pin and INV in order to fix narrow bandwidth and avoid high distortion of the input current waveform. In this way a

voltage value (VCOMP) is determined, it is the reference (in the multiplier characteristic graph) for the “MULT” and “CS” signal. Taking this into account, the procedure to set the operation point of the multiplier Pin3 (MULT) is suggested. First, the maximum peak value is selected. This value, which occurs at maximum mains voltage, should be less 3 V in case of single mains. Therefore:

- Minimum peak value: $V_{MULTpk\min} = V_{MULTpkx} \frac{V_{INRMS\min}}{V_{INRMS\max}}$
- This value is then multiplied by the minimum guaranteed $\frac{\Delta V_{CS}}{\Delta V_{MULT}} = 1.1$ and it gives

$$\text{the maximum output voltage of multiplier: } V_{CSpk} = 1.1 * V_{MULTpkx \min} .$$

- In this way the divider resistor is: $\frac{R_3}{R_1 + R_2 + R_3} = \frac{V_{MULTpkx}}{\sqrt{2} * V_{INRMS\max}}$.
- Subsequently thanks to these relationships: $V_{CS} = k(V_{COMP} - 2.5V)V_{MULT}$

$$R_S < \frac{V_{CS\min}}{IL_{peak}} .$$

The divider resistor $R3=15\text{ k}\Omega$ and $R1/R2=2.7\text{ M}\Omega$ and the sense resistors $R9=0.39\text{ }\Omega$ and $R10=1\text{ }\Omega$ have been fixed.

In particular:

- the reference for the current sense.
- the typical multiplier gain
- the voltage on the Pin2
- the voltage on the Pin3

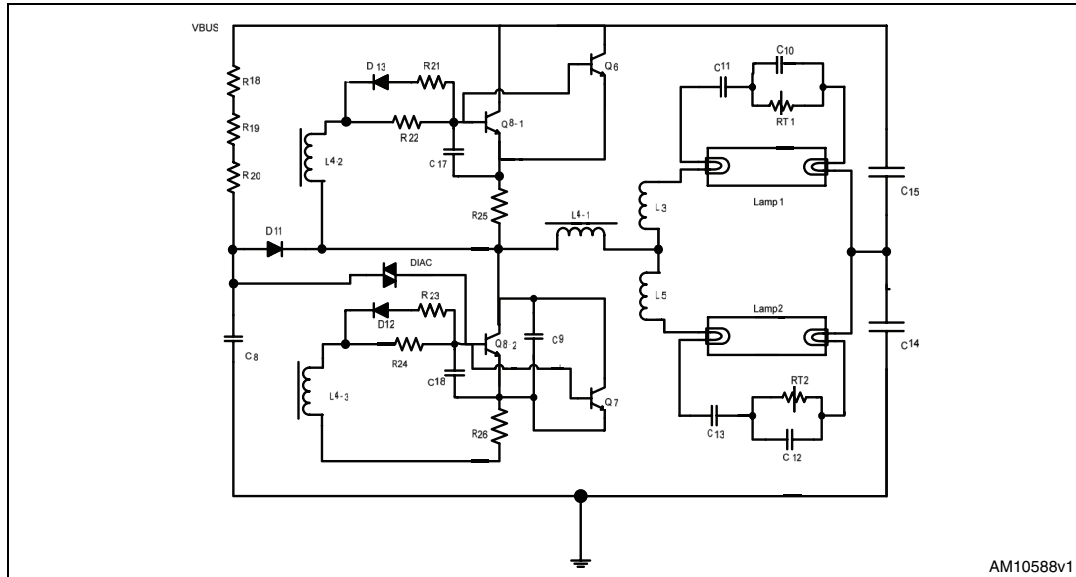
This experimental fine tuning guarantees a high value of both PF and THD.

Pin5 (ZCD).This pin is the zero current detector circuit. In this case (PFC in transition mode) the ZCD pin is connected, through a resistor, to the auxiliary winding of the boost inductor. In particular, the resistance value ($R6=47\text{ k}\Omega$) was tuned in order to minimize the switching power losses at turn-on. In fact, this fine tuning allows the MOSFET to switch on when the resonant phenomenon between boost inductor and drain-source capacitance occurs on the valley of the drain voltage. In this way, the MOSFET device turns on with lower voltage across drain source, this implies a reduced current peak and lower switch-on losses.

3 DC-AC converter

The electronic ballast consists of a self-oscillating voltage-fed half bridge inverter, which has been developed to drive two lamps of 28 W. One of the key components is the STD845DN40 power bipolar transistor. It is a dual NPN high voltage power transistor and is housed in dual-island DIP-8 package. This package solution allows to save layout area and its driving circuit has been optimized so that the thermal performance is not too different to that of a single transistor. The second of the key components is the possibility to use, for bipolar transistors, a DIP-8 or SOT-82 package solution.

Figure 5. DC-AC converter section



The DC-AC converter section has been realized according to customer indications. The ballast coil L3/L5 (3.7 mH) and the saturable core transformer L4 (20 μ H) were given by the customer and in relation to this, all the other passive and active elements have been selected. In particular, the design has been realized so that the lamp voltage is 180 V and the lamp current about 0.15 A. The following design procedure is suggested for resonant components and for proper operation of the self-oscillating inverter.

Considering first the given set of specifications: $V_{BUS}=400$ V, output current $I_{OUT}=0.15$ A, ballast coil $L3/L5=3.7$ mH, core saturable transformer $L4=20$ μ H and, more specifically, the lamp resistance ($R \approx 1160 \Omega$).

The RMS input voltage can be calculated from:

Equation 2

$$V_{IN_RMS} = V_{BUS} \frac{\sqrt{2}}{\pi}$$

The value of the desired characteristic impedance is extracted:

Equation 3

$$Z_r = \sqrt{\frac{L}{C}} = \frac{V_{IN_RMS}}{I_{OUT}}$$

Given the resonance inductance, the switching frequency is calculated:

Equation 4

$$f_s = \frac{Z_r}{2\pi L_3}$$

Then the resonant capacitor is given by:

Equation 5

$$C_r = \frac{1}{2\pi f_s * Z_r}$$

where $C_r = C10 + C11$.

For proper operation resonant, the network must be $Q = \frac{R}{Z_r} > 1$, in this way the

drop across the serially connected lamps is higher than the bus voltage and the current is sinusoidal. This is the preferred operation mode.

3.1 System description

The system description is subdivided into three main sections, preheating, ignition and steady-state phase.

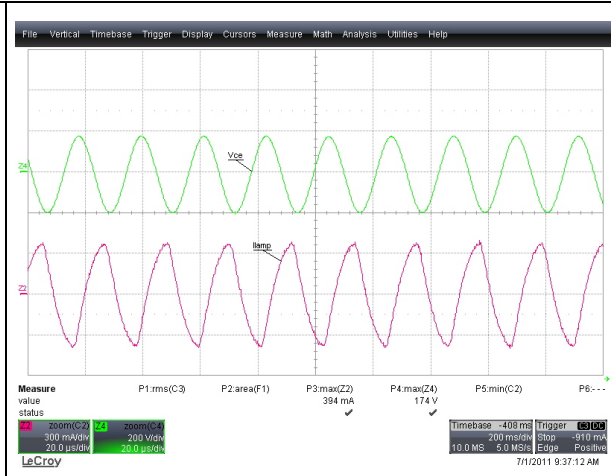
3.1.1 Preheating phase

To obtain a long lamp life, it is important that the electrodes are preheated by a certain current. A PTC RT1 (for the single lamp) put in parallel with the lamp guarantees the electrode preheating as it ensures that the current is flowing via the lamp electrodes. During this period the voltage across the lamp is maintained sufficiently low to avoid the lamp igniting too early and the operating frequency is determined by L3 and C11 (C10 is partially inhibited by PTC).

Figure 6. Voltage and current lamp waveforms



Figure 7. Zoom of the highlighted section (in Figure 6)



The preheating time depends on the setting of the circuit parallel to the lamp (time constant). In particular, it is the PTC value that determines this duration of preheating as well as the ignition of the lamp. In fact, as long as it does not increase its impedance, it does not allow the resonant circuit (L3, C11, and C10) to generate the overvoltage on the lamp and so on the ignition itself.

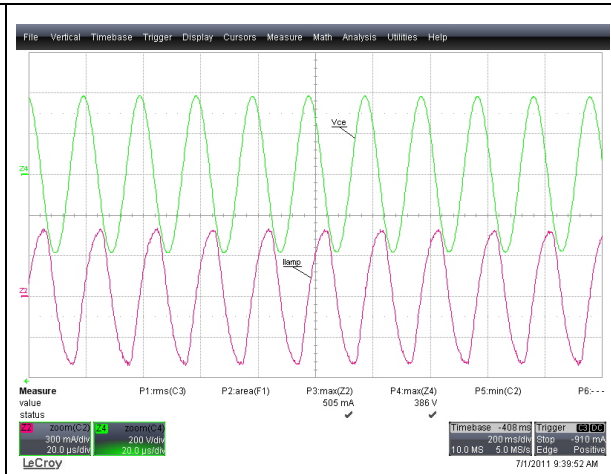
3.1.2 Ignition phase

As soon as the electrodes are preheated, the impedance of the PTC rapidly increases and the series resonance of L3, C11, and C10 results in an increasing lamp voltage. The lamp voltage increases until it ignites.

Figure 8. Voltage and current lamp waveforms



Figure 9. Zoom of the highlighted section (in Figure 8)



The resonant circuit operates in order to ignite the lamp. In the ignition phase, the voltage shape of the lamp depends on the rise time of the PTC impedance.

Resonant circuit frequency:

Equation 6

$$f_r = \frac{1}{2\pi\sqrt{L_3(C_{10} + C_{11})}}$$

3.1.3 Steady-state phase

Once the tubes are ionized, it is effectively a short-circuit across $C_{10} + C_{11}$. The inverter system sets the voltage and current shape so that the lamp correctly operates.

Figure 10. Voltage and current lamp waveforms



Figure 11. Zoom of the highlighted section (in Figure 10)



Therefore, the frequency is defined by C_{15} and so is lower than the ignition phase. At this frequency, the overvoltage generated is also lower, but enough to keep the tube lit. During steady-state, when the transistor is first turned on, the current in the transformer L_4 increases until its core saturates. At this point, after the storage time of the transistor has passed, it turns off. In this way, the operating frequency also depends on the size and maximum flux density of the core of L_4 and the storage times of the transistor.

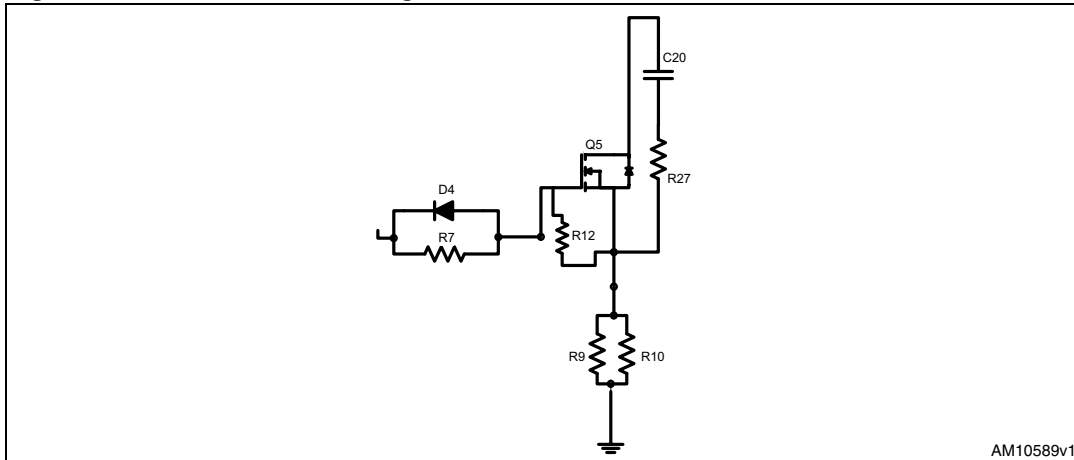
4 Driving optimization

The driving circuit optimization has been done in order to have the best performance of the lighting system. Basically, this circuit concerns MOSFET and BJT transistors and it has been realized in order to have thermal and electrical behavior of devices compliant to the system features.

4.1 MOSFET circuit optimization

The elements of circuit optimization are shown below.

Figure 12. Snubber and driving circuit of MOSFET



A small RC snubber circuit ($C=680\text{ pF}$ and $R=180\Omega$) has been used to prevent voltage spikes and voltage oscillation across the MOSFET during device turn-off. This means limiting the rate of rise ($\Delta V_{DS}/\Delta t$) of the MOSFET, to reduce the cross between voltage and current and to have less switching losses during turn-off. The driving circuit ($R7=47\Omega$ and diode) allows the MOSFET to not turn on too quickly in order to reduce the discharge of snubber circuit capacitance and consequently to guarantee negligible switch-on losses and, thanks to the diode, it allows the fastest discharge of parasitic capacitance of the MOSFET and therefore speeds up switch-off.

The waveforms show the advantages of the driving solution and the snubber circuit.

Figure 13. MOSFET turn-off without snubber circuit

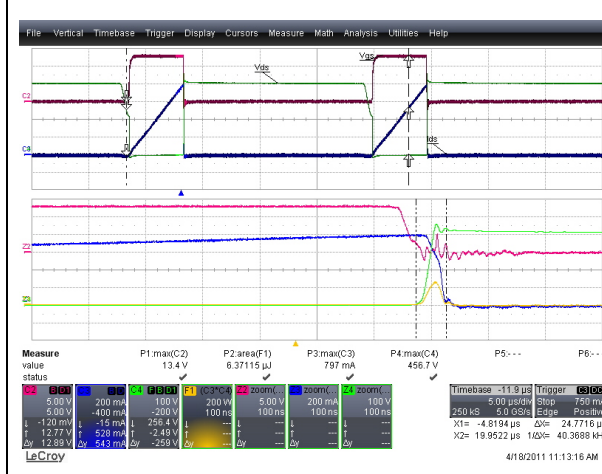
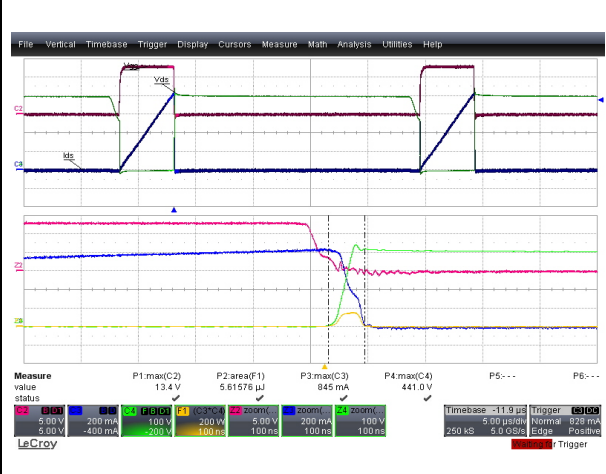


Figure 14. MOSFET turn-off with snubber circuit



The comparison between these waveforms shows that the insertion of the RC snubber circuit reduces voltage spikes and Vds slope and in particular it decreases switching losses during turn-off.

Figure 15. MOSFET turn-on @ R7=10 Ω

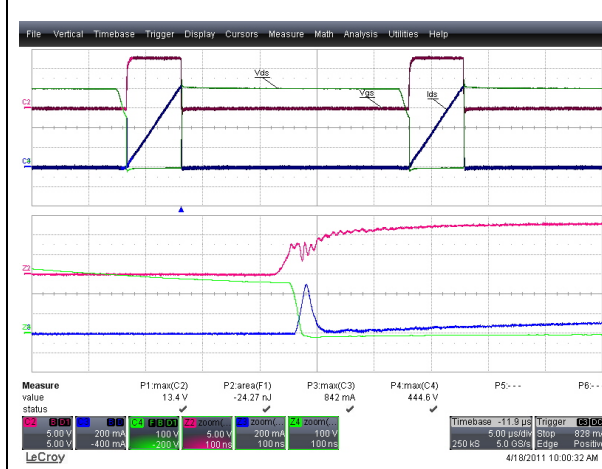
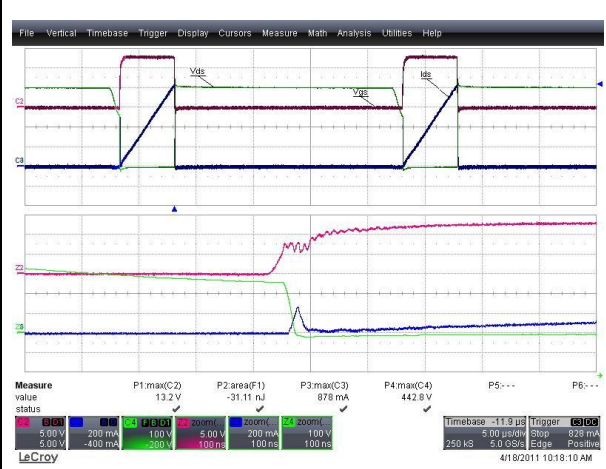


Figure 16. MOSFET turn-on R7=47 Ω

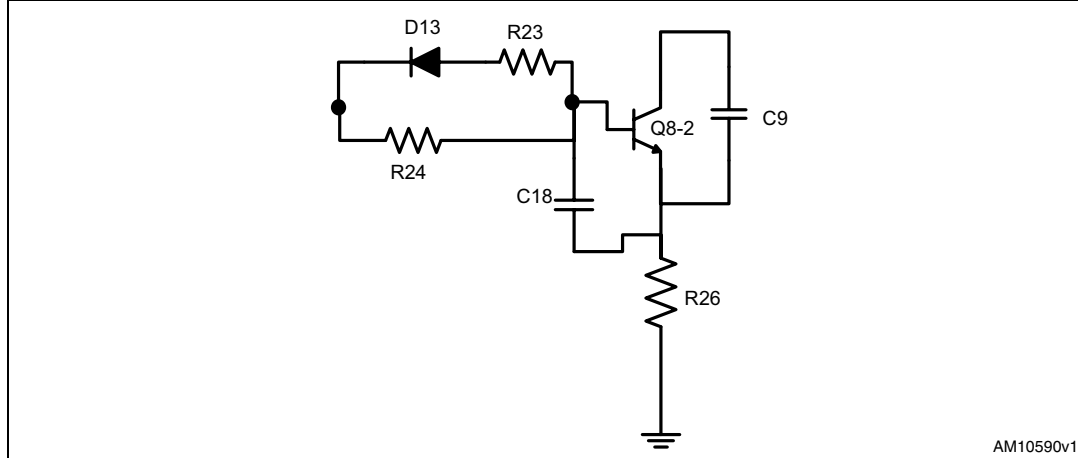


As the figures show, the resistor R7=47 Ω in the driving circuit provides a slower switch-on of the MOSFET, reduces the discharge of snubber circuit capacitance and consequently it guarantees negligible power losses during turn-on.

4.2 BJT circuit optimization

The snubber and the driving circuit of BJT is the same as low side and high side. In particular, [Figure 6](#) shows the elements of low side BJT driving circuit which are highlighted.

Figure 17. BJT in low side. Snubber and driving circuit of BJT



AM10590v1

A small C9 snubber circuit has been used in order to decrease the cross between voltage (VCE) and current (ICE) and, consequently, to have less switching losses during turn-off. The capacitance C9 allows to limit, in the middle point (2), the rate of rise of VCE. This snubber capacitance is put in the low side in order to ensure the discharge to ground and therefore to avoid a current too high spike during the startup phase. The choice of the C9 capacitance was made in order to balance the power switching losses, in fact, the value C9=680 pF, obtained in experimental results, guaranteed the lowest switch-off losses and negligible switch-on losses due to the discharge of capacitance during the turn-on of the transistor. The driving circuit ($R_{23}=5.6\ \Omega$, $R_{24}=33\ \Omega$ and diode) provided the best commutation of the bipolar transistor. The R_{24} value was able to reduce current spike due to the discharge of snubber circuit capacitance and to ensure the charge quantity so that the IC current was sufficient to power the lamp. $R_{23}||R_{24}$ put in parallel determined the commutation time, the storage time of the bipolar transistor, and consequently the operating frequency of the ballast system.

The waveforms in [Figure 18](#) show the behavior of BJT during steady-state operation.

Figure 18. Steady-state operation

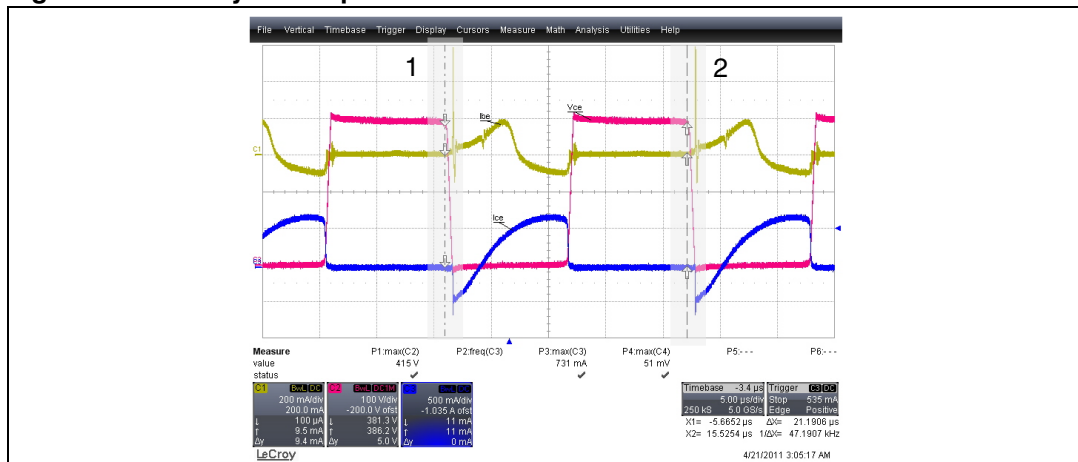


Figure 19. Zoom of the highlighted section 1
(in [Figure 18](#))

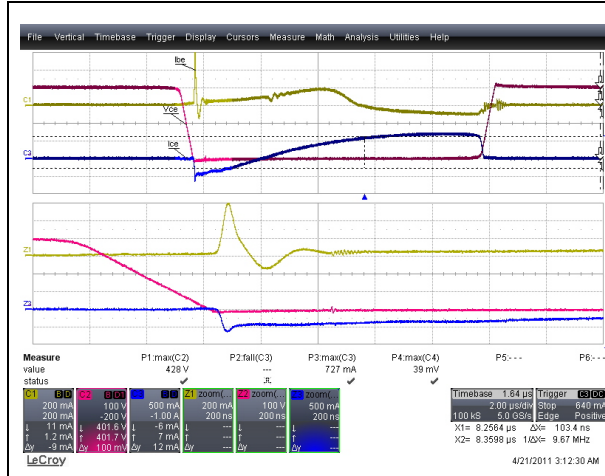
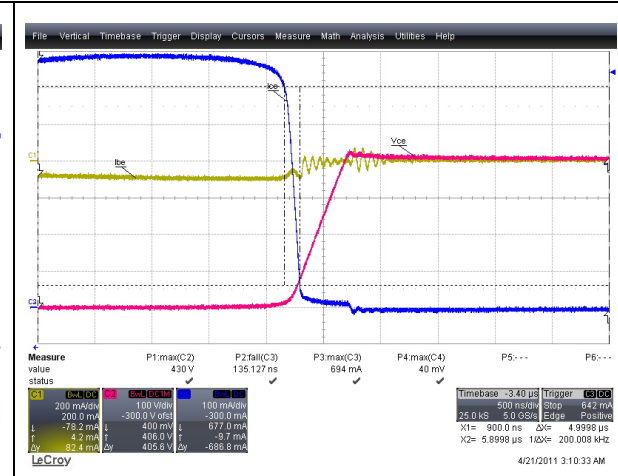


Figure 20. Zoom of the highlighted section 2
(in [Figure 18](#))



The turn-on of the bipolar transistor had a spike of I_{be} current due to C_{18} capacitance, it assisted the charge phenomenon of the bipolar junction. The fall time value during the turn-off was very low and this implied shorter commutation time and lower switching losses.

5 Experimental results

The experimental results have been measured for different input voltage levels and leaving the application in free air: all electrical components were in the original position. The test equipment list has been given in order to check the measurements repeatability.

- Input voltage: ~180 - 230 - 265 Vac
- Test equipment:
 - Agilent AC power supply 6813B
 - Digital power meter WT210
 - Flir systems thermal camera
- Ambient temperature:
 - ~25 °C

Table 2. Main electrical and thermal results @ 25 °C ambient temperature

| Input voltage [V] | PFC | THD | Pin [W] | MOSFET temperature [°C] | BJT temperature [°C] @ DIP-8 |
|-------------------|-------|------|---------|-------------------------|------------------------------|
| 180 V | 0.998 | 3.5 | 66.4 | 52 | 78 |
| 230 V | 0.993 | 4.1 | 65.4 | 43 | 78 |
| 264 V | 0.983 | 13.9 | 65.8 | 42 | 78 |

Exchanging input voltage, the main electrical parameters of the PFC factor and THD suggest that the application performances were very good. Everything the energy soaked up by the system was converted into useful power. The temperatures of transistor devices respect the datasheet specifications. In particular the temperature of BJT transistors was not too high considering that the DIP-8 package had a dual NPN high voltage power transistor housed in dual-island.

In [Table 3](#), the thermal performance between the DIP-8 and SOT-82 package were compared.

Table 3. Thermal results @ 25 °C ambient temperature

| Input voltage [V] | BJT temperature [°C] @ DIP-8 | BJT temperature [°C] @ SOT-82 |
|-------------------|------------------------------|-------------------------------|
| 230 V | 78 | 61 |

The temperature of the two package solutions was not too different, for both cases the transistors worked in safety condition. The temperature value of the bipolar transistor didn't depend on the input voltage because the PFC active section allows to fix, at 400Vdc, the voltage of the DC-AC section. For this reason the temperature of the bipolar (both packages), was only measured at 230 Vac (nominal input voltage).

6 Conclusions

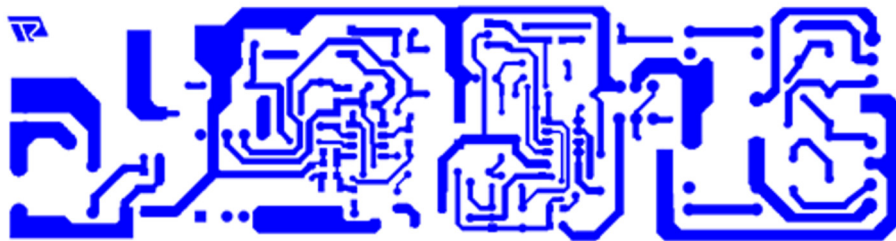
The proposed design of electrical ballast with active PFC and self-oscillating inverter showed the capability of driving 2X28 W fluorescent lamps with very good electrical and thermal performance. The component choice and the optimization of the transistors driving circuit guarantee the highest PFC factor and lowest THD. For each work condition the ballast drove the lamps safely.

This power source offers the customer the double package solution: bipolar transistors in DIP-8 or SOT-82 package. For both solutions the temperature of power devices is fully compliant with the absolute maximum rating limit in the datasheet specification.

In addition, the design layout was designed using the double layer solution. Anyway, according to customer needs, the PCB layout of the application can be realized both in double layer and in single, using the jumpers instead of the net in the top layer.

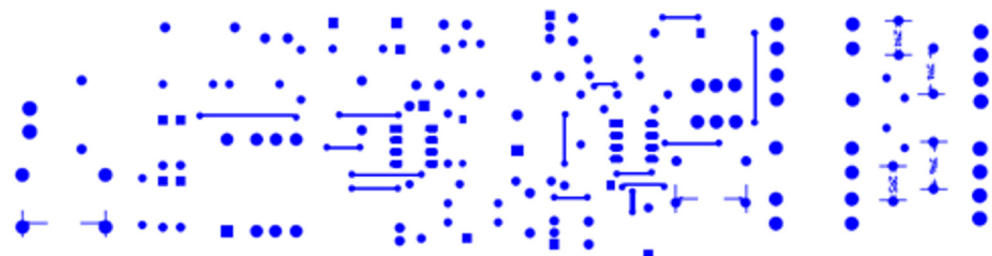
7 Layout layers

Figure 21. Bottom layout layer



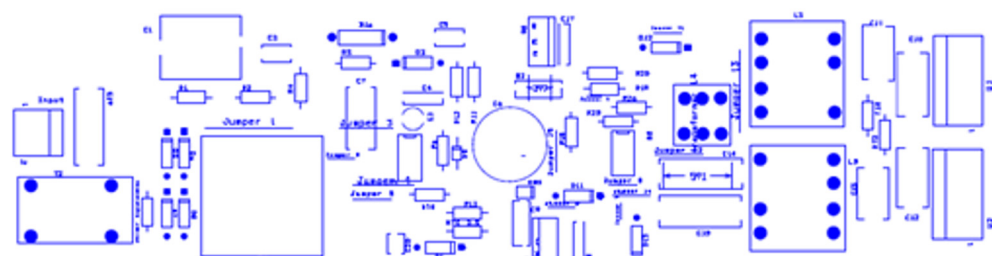
AM10591v1

Figure 22. Top layout layer



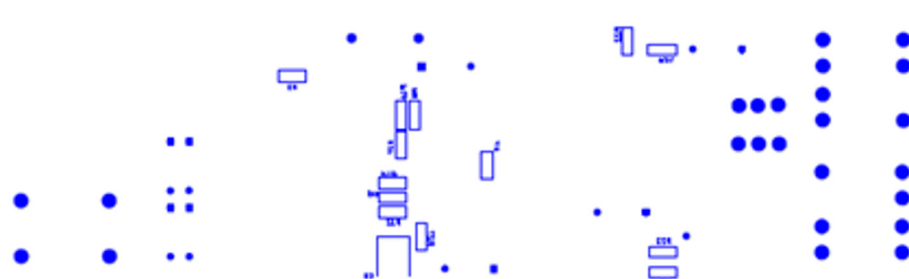
AM10592v1

Figure 23. Silkscreen top



AM10593v1

Figure 24. Silkscreen bottom



AM10594v1

8 Bill of material

Table 4. Bill of material

| Quantity | Reference | Part/value |
|----------|--------------------|------------|
| 2 | R1/R2 | 2.7 MΩ |
| 1 | R3 | 15 kΩ |
| 2 | R4/R5 | 270 kΩ |
| 1 | R6 | 47 kΩ |
| 1 | R7 | 10 Ω |
| 1 | R12 | 47 kΩ |
| 1 | R9 | 0.39 Ω |
| 1 | R10 | 1 Ω |
| 2 | R11/R12 | 220 Ω |
| 2 | R13/R14 | 1 MΩ |
| 1 | R15 | 15 kΩ |
| 1 | R16 | 82 kΩ |
| 1 | R17 | 10 kΩ |
| 3 | R18/R19/R20 | 180 kΩ |
| 2 | R21/R23 | 5.6 Ω |
| 2 | R22/R24 | 33 Ω |
| 2 | R25/R26 | 0.82 Ω |
| 1 | R27 | 180 Ω |
| 1 | C1 | 150 nF |
| 4 | C2/C5/C17/C18 | 10 nF |
| 1 | C3 | 10 µF |
| 2 | C4/C8 | 100 nF |
| 1 | C6 | 33 µF |
| 1 | C7 | 1 µF |
| 1 | C21 | 680 pF |
| 2 | C10/C12 | 4.7 nF |
| 2 | C11/C13 | 10 nF |
| 2 | C14/C15 | 100 nF |
| 1 | C20 | 27 pF |
| 1 | C19 | 330 nF |
| 1 | Filter capacitance | 2.2 nF |
| 1 | D1 | STTH1L06A |

Table 4. Bill of material (continued)

| Quantity | Reference | Part/value |
|----------|-----------------|-------------------------|
| 4 | D3/D4/D12/D13 | 1N4148 |
| 5 | D5/D6/D7/D8/D11 | 1N4007 |
| 1 | D16 | Zener |
| 2 | RT1/RT2 | PTC |
| 1 | NTC | 2.5 |
| 1 | T2 | 18 mH filter inductance |
| 1 | T1 | 1.8 mH 0.5 A |
| 1 | L4 | 20 µH |
| 2 | L3/L5 | 3.7 mH |
| 1 | U3 | L6562A |
| 1 | Q1 | STD3N62K3 |
| 1 | Q8 1-2 bipolar | STD845DN40 |

9 Reference

1. AN2761 application note

10 Revision history

Table 5. Document revision history

| Date | Revision | Changes |
|-------------|----------|------------------|
| 11-Nov-2011 | 1 | Initial release. |

Please Read Carefully:

Information in this document is provided solely in connection with ST products. STMicroelectronics NV and its subsidiaries ("ST") reserve the right to make changes, corrections, modifications or improvements, to this document, and the products and services described herein at any time, without notice.

All ST products are sold pursuant to ST's terms and conditions of sale.

Purchasers are solely responsible for the choice, selection and use of the ST products and services described herein, and ST assumes no liability whatsoever relating to the choice, selection or use of the ST products and services described herein.

No license, express or implied, by estoppel or otherwise, to any intellectual property rights is granted under this document. If any part of this document refers to any third party products or services it shall not be deemed a license grant by ST for the use of such third party products or services, or any intellectual property contained therein or considered as a warranty covering the use in any manner whatsoever of such third party products or services or any intellectual property contained therein.

UNLESS OTHERWISE SET FORTH IN ST'S TERMS AND CONDITIONS OF SALE ST DISCLAIMS ANY EXPRESS OR IMPLIED WARRANTY WITH RESPECT TO THE USE AND/OR SALE OF ST PRODUCTS INCLUDING WITHOUT LIMITATION IMPLIED WARRANTIES OF MERCHANTABILITY, FITNESS FOR A PARTICULAR PURPOSE (AND THEIR EQUIVALENTS UNDER THE LAWS OF ANY JURISDICTION), OR INFRINGEMENT OF ANY PATENT, COPYRIGHT OR OTHER INTELLECTUAL PROPERTY RIGHT.

UNLESS EXPRESSLY APPROVED IN WRITING BY TWO AUTHORIZED ST REPRESENTATIVES, ST PRODUCTS ARE NOT RECOMMENDED, AUTHORIZED OR WARRANTED FOR USE IN MILITARY, AIR CRAFT, SPACE, LIFE SAVING, OR LIFE SUSTAINING APPLICATIONS, NOR IN PRODUCTS OR SYSTEMS WHERE FAILURE OR MALFUNCTION MAY RESULT IN PERSONAL INJURY, DEATH, OR SEVERE PROPERTY OR ENVIRONMENTAL DAMAGE. ST PRODUCTS WHICH ARE NOT SPECIFIED AS "AUTOMOTIVE GRADE" MAY ONLY BE USED IN AUTOMOTIVE APPLICATIONS AT USER'S OWN RISK.

Resale of ST products with provisions different from the statements and/or technical features set forth in this document shall immediately void any warranty granted by ST for the ST product or service described herein and shall not create or extend in any manner whatsoever, any liability of ST.

ST and the ST logo are trademarks or registered trademarks of ST in various countries.

Information in this document supersedes and replaces all information previously supplied.

The ST logo is a registered trademark of STMicroelectronics. All other names are the property of their respective owners.

© 2011 STMicroelectronics - All rights reserved

STMicroelectronics group of companies

Australia - Belgium - Brazil - Canada - China - Czech Republic - Finland - France - Germany - Hong Kong - India - Israel - Italy - Japan - Malaysia - Malta - Morocco - Philippines - Singapore - Spain - Sweden - Switzerland - United Kingdom - United States of America

www.st.com